Journal of Power Sources 548 (2022) 232071

Contents lists available at ScienceDirect

Journal of Power Sources

journal homepage: www.elsevier.com/locate/jpowsour

Flexible and freestanding PANI: PSS/CNF nanopaper electrodes with enhanced electrochemical performance for supercapacitors

Yue Liang [a], Zhen Wei [b], Hung-En Wang [a], Martin Flores [a], Ruigang Wang [b,**], Xinyu Zhang [a,*]

[a] Department of Chemical Engineering, Auburn University, Auburn, AL, 36849, USA
[b] Department of Metallurgical and Materials Engineering, The University of Alabama, Tuscaloosa, AL, 35487, USA

HIGHLIGHTS

- Freestanding, binder-free flexible nanopaper electrode was successfully fabricated.
- Electrode with excellent flexibility, cycling stability and mechanical property.
- Symmetric supercapacitor device delivered high areal capacitance and energy density.
- Great potential for next-generation green-economy portable and wearable electronics.

ARTICLE INFO

Keywords:
Cellulose nanopaper
Conducting polymer
Flexible electrode
Supercapacitor

ABSTRACT

With the fast-expanding markets of portable and wearable electronics, the development of sustainable, cost-effective, and flexible electrodes for energy storage applications is critical. Herein, a flexible, freestanding, binder-free polyaniline: poly (sodium 4-styrene sulfonate)/cellulose nanopaper (PANI: PSS/CNP) electrode was prepared using an in situ polymerization with a facile vacuum filtration approach. The low-cost and environmentally friendly nanocellulose with a three-dimensional (3D) hierarchical porous structure was chosen as the substrate that not only reduced the production cost but also improved the electrolyte absorption, flexibility, and mechanical strength for PANI: PSS/CNP. The freestanding and binder-free structure simplifying the preparation process and increasing the mass loading of the active material in the electrode was beneficial to maximizing electrode utilization. Due to the effective combination of cellulose and PANI: PSS complex, PANI: PSS/CNP electrode exhibited high specific capacitance (2.56 F/cm^2) with excellent cycling stability (81.5% capacitance retention, 8000 cycles), mechanical strength, conductance stability, and flexibility. A symmetric supercapacitor device was constructed with PANI: PSS/CNP electrodes, showing outstanding areal specific capacitance (460 mF/cm^2) and high energy density (40.9 μWh/cm^2). Our work offers a novel and economical approach for the future production of sustainable, low-cost, and energy-efficient flexible electrode materials.

1. Introduction

With rapidly growing industries and markets for portable and wearable consumer electronics, such as foldable displays, electronic skin, and electric paper, the demand for flexible and renewable energy storage devices with low cost, lightweight, environmental friendliness, and superior energy efficiency is clearly increasing [1–4]. Among various energy storage devices, flexible supercapacitors have been widely recognized as promising candidates due to their high power density, long cycling life, robust mechanical flexibility, and good operational safety [5–9]. As the most important part of flexible supercapacitors, the flexible electrode is considered as a key impact on the successful fabrication of high performance flexible supercapacitors.

Polyaniline (PANI) as a promising electrode material has been extensively studied in supercapacitors due to its high specific capacitance, easy and simplistic preparation, easy control of doping level and conductivity, good environmental stability, and low cost [10,11]. However, the weak solubility in common solvents, structural instability, and poor mechanical performance limit its applications in flexible electronic devices. A common method used to overcome the insolubility

* Corresponding author.
** Corresponding author.
E-mail addresses: rwang@eng.ua.edu (R. Wang), xzz0004@auburn.edu (X. Zhang).

https://doi.org/10.1016/j.jpowsour.2022.232071
Received 30 June 2022; Received in revised form 29 August 2022; Accepted 3 September 2022
Available online 14 September 2022
0378-7753/© 2022 Elsevier B.V. All rights reserved.

problem of conducting polymers is to combine polymeric surfactants with different sulfonating groups and conducting polymer to form complexes [12,13]. For instance, polyaniline: poly (sodium 4-styrene sulfonate) (PANI: PSS) with excellent solution-processability and unique redox behaviors has been widely applied in supercapacitors. A hybrid electroactive material formed by iron oxide-decorated few-layer graphene/PANI: PSS composite films through a simple dip-coating procedure showed excellent capacitive performance [14]. The "sandwich-like" nanocomposites multiwalled carbon nanotubes/polyaniline/poly (sodium 4-styrenesulfonate)-graphene (MWCNTs/PANI/PSS-GR) demonstrated a high specific capacitance [15]. In addition, extensive work has been done to modify and improve the electrochemical performance of PANI, such as preparing different morphologies of PANI, making composites with carbon-based materials, and depositing active conducting materials on flexible, porous, and light-weight substrates [16–21].

Cellulose nanofibrils (CNFs), the most abundant natural polymer on earth, has received great attention, in light of its abundant and renewable raw materials source, high surface area, superior mechanical strength, non-toxicity, great biocompatibility and biodegradability, and prospects for environmental sustainability, etc. [22] The three-dimensional (3D) hierarchical porous structures of cellulose formed through intramolecular and intermolecular hydrogen bonds among cellulose molecules provide rich ion absorptive sites and more diffusion channels for charge transfer, which is beneficial for enhancing the performance of supercapacitors [23]. Furthermore, the hydroxyl groups can be easily modified and provide a good platform for the construction of new materials to broaden their potential applications. Compared to other flexible substrates, CNFs is widely regarded as an ideal building block to reduce production costs and build environmentally friendly processes for the fabrication of the functional flexible electrodes. A series of cellulose-based functional materials have been fabricated and applied in flexible energy storage devices. For example, Deng et al. prepared multiwalled carbon nanotube (MWNT)/activated cellulose (ACNF) whose capacitance was 1.38 times higher than that of pure ANCF, when adding 6 wt% MWNTs in CNFs. In addition, 94% initial capacitance was retained over 1000 cycles at the current density of 2 A/g [24]. Uniform cellulose/graphene/polypyrrole (CNF/GN/PPy) microfibers were prepared with a convenient wet-spinning strategy. This microfiber electrode manifested excellent tensile strength (364.3 MPa), high specific capacitance (334 mF/cm^2), and good cycling stability (capacitance retaining nearly 100% after 2000 charge-discharge cycles) [25].

In this study, we aim to develop a sustainable and inexpensive strategy to synthesize flexible electrodes with high electrochemical performance to meet the requirements of global markets for flexible and renewable energy storage devices. Here, we designed and prepared a new freestanding, binder-free flexible polyaniline: poly (sodium 4-styrene sulfonate)/cellulose nanopaper (PANI: PSS/CNP) electrode through in situ polymerization and a fast vacuum filtration method, which combines the solution-processable PANI: PSS complexes as the active material with CNFs as the flexible substrate. The cheap and green CNF as a substrate not only effectively reduces the production cost but also improves the flexibility and mechanical strength of electrodes. The optimized PANI: PSS/CNP electrode exhibited high tensile strength, where the sample strips (10 mm wide and 0.1 mm thick) could still lift a static load of 800 g. The freestanding and binder-free construction eliminates the need for binders, conductive additives, and current collectors while simplifying the preparation process and increasing the mass loading of the active material in the electrode, and maximizing electrode utilization. The optimized PANI: PSS/CNP demonstrated a high areal specific capacitance of 2.56 F/cm^2 and good cycling stability (81.5% capacitance retention, 8000 cycles). A symmetric supercapacitor assembled with two pieces of PANI: PSS/CNP electrodes delivered a high areal energy density of 40.9 μWh/cm^2 (4.09 mWh/cm^3) at a power density of 100.5 μW/cm^2 (10.05 mW/cm^3). This research opens a new avenue for developing low-cost freestanding flexible electrodes of supercapacitors.

2. Experiments

2.1. Materials

The CNFs with a concentration of about 3 wt% were purchased from the University of Maine, USA. (Lot Number U31). Aniline monomer (99%) and ammonium peroxydisulfate (APS, 98%) were purchased from Alfa Aesar. Poly (sodium-4-styrenesulfonate) (PSS, 99%) was purchased from Acros, USA. Sulfuric acid (H_2SO_4, 95%–98%) and hydrochloric acid (HCl, 36.5%–38%) were purchased from VWR, USA. All chemicals were directly used without further purification.

2.2. Preparation of cellulose nanopaper (CNP)

The preparation of CNP was carried out according to our previous work [26]. In short, the suspension of CNFs with a concentration of 0.5 wt% was diluted by 1 M HCl. The diluted suspension of CNFs (40 ml) was magnetically stirred for 2 h to obtain a uniform suspension. Then, the suspension was filtered using a polypropylene filter membrane (diameter of 10 cm, pore size of 0.45 μm) by a vacuum filtration method. Finally, another polypropylene filter membrane was covered on the wet CNFs film and dried at 105 °C for 2 h to obtain the CNP.

2.3. Preparation of PANI: PSS/CNP

40 ml of CNFs suspension (0.5 wt%) was dispersed in 1 M HCl (20 ml) and stirred for 30 min to form a homogeneous suspension. Then the aniline monomer and PSS were introduced to the suspension and stirred for another 10 min. Next, the oxidant of APS was added into the mixture to initiate the polymerization of aniline. The reaction was carried out for 3–4 h under constant magnetic stirring at room temperature. The resultant solid was centrifuged and washed several times with deionized water. After that, the product was diluted to 200 ml with deionized water and sonicated for 5 min at a power input of 500 W. Finally, the PANI: PSS/CNF suspension was filtered by vacuum filtration using a polypropylene filter membrane (diameter of 10 cm, pore size of 0.45 μm). The PANI: PSS/CNP was obtained by drying the wet PANI: PSS/CNF film that was covered by another polypropylene filter membrane at 105 °C for 2 h. The schematic of forming the PANI: PSS/CNP is shown in Scheme 1, where PSS acts as a surfactant as well as a dopant in the composite. The weight percentage of PANI: PSS in the PANI: PSS/CNP was calculated following Eq. (1):

$$\text{Weight ratio} = (m - 0.2/m) \times 100\% \quad (1)$$

where m is the dry weight (g) of the PANI: PSS/CNP.

To obtain optimal performance of composites, the weight ratio of PANI: PSS in PANI: PSS/CNP was accurately controlled. The detail is given in Table 1.

2.4. Tensile test

The mechanical properties of PANI: PSS/CNP samples were examined by the TA Instrument dynamic mechanical analyzer RSA III with the ASTM standard D882-18 test method. The specimens were cut into the 1 cm (width) × 5.5 cm (length) segments used to test. The crosshead speed and gauge length were 6 mm/min and 15 mm, respectively. Three measurements data were averaged to obtain the value for each sample.

2.5. Conductivity measurement

The electric conductivity (ρ, S/cm) of PANI: PSS/CNP was examined by the four-point probe method using a digital multimeter (RIGOL

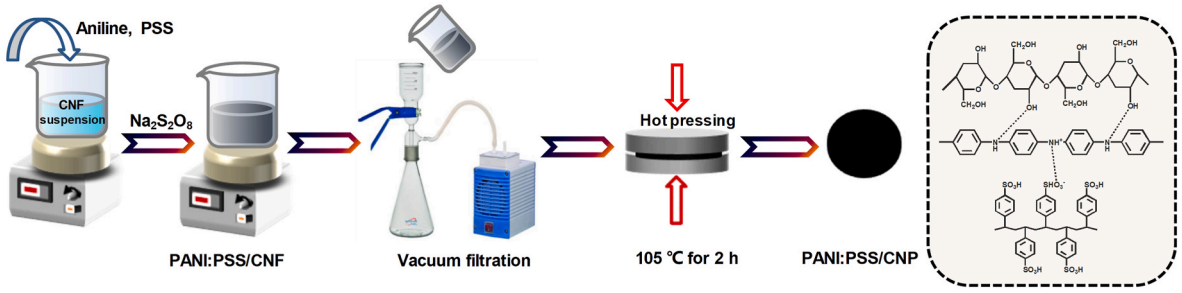

Scheme 1. Schematic formation of PANI: PSS/CNP.

Table 1
Operation conditions for the synthesizing of PANI: PSS/CNP.

Sample	CNF (g)	Aniline (ml)	PSS (g)	APS (g)	Weight ratio of PANI: PSS (%)
PANI: PSS/CNP-1	0.2	0.1	0.0097	0.228	7.7 ± 0.3
PANI: PSS/CNP-2	0.2	0.2	0.0194	0.456	29.0 ± 0.8
PANI: PSS/CNP-3	0.2	0.3	0.0291	0.684	46.8 ± 1.2
PANI: PSS/CNP-4	0.2	0.4	0.0388	0.912	54.1 ± 1.5
PANI: PSS/CNP-5	0.2	0.5	0.0483	1.140	62.2 ± 1.8

DM3068) and calculated by Eq. (2) [27],

$$\rho = 1/(R_s \times t) \quad (2)$$

where R_s is the sheet resistance in Ohm, which is the average value after five square specimens (1 × 1 cm^2) measured for each sample. t is the thickness of the film in centimeter.

2.6. Electrochemical measurements

All electrochemical tests were carried out on a CHI electrochemical workstation (CHI 760D) using three-electrode or two-electrode system in 1 M H_2SO_4. The reference electrode, the counter electrode, and the working electrode were Ag/AgCl electrode, platinum sheet (1 × 1 cm^2), and PANI: PSS/CNP (1 cm × 1 cm × 0.10 mm, 11 mg), respectively. Cyclic voltammetry (CV) and galvanostatic charge/discharge (GCD) curves were conducted with a potential window from 0 to 0.8 V. The PANI: PSS/CNP electrode (1 cm × 1 cm × 0.10 mm, 11 mg) was employed as cathode and anode to build the symmetric supercapacitor. Electrochemical impedance spectra (EIS) were obtained at open-circuit voltage using an AC amplitude of 0.005 V in the frequency range of 10^{-1} to 10^5 Hz. The stability tests were performed on Arbin Instrument (version 4.21). The areal specific capacitance (C_A, F/cm^2) of the electrode was estimated by Eq. (3) from the GCD curves [28],

$$C_A = I\Delta t/A\Delta V \quad (3)$$

where I is the discharge current (A), Δt is discharge time (s), A is the area of the electrode (cm^2), and ΔV is the potential window (V). When the area in the formula is replaced by the volume or mass of the electrode, the gravimetric capacitance (C_g, F/g) and the volumetric capacitance (C_V, F/cm^3) will be obtained.

The energy density (E, Wh/cm^2) and power density (P, W/cm^2) were calculated according to the following Eqs. (4) and (5):

$$E = C\Delta V^2/(2 \times 3600) \quad (4)$$

$$P = (3600 \times E)/\Delta t \quad (5)$$

3. Materials characterization

Scanning electron microscopy (SEM; Apreo FE) and energy dispersive X-ray spectroscopy (EDS; EDAX Instruments) were used to confirm the morphologies and compositional elements of the samples, respectively. The function groups were investigated by Fourier transform infrared spectroscopy (FTIR) on a Nicolet 6700 using a KBr disk in the region of 400–4000 cm^{-1}. X-ray photoelectron spectroscopy (XPS, Kratos XSAM 800) was used to determine the elemental valence state of the samples.

4. Results and discussions

4.1. Material characterization

Structural characterization of CNP, PANI: PSS, and PANI: PSS/CNP were investigated by FTIR as shown in Fig. 1. Pure CNP exhibited a few peaks including the bending mode of the absorbed water at 1645 cm^{-1}, symmetric bending of –CH_2 at 1430 cm^{-1}, O–H bending at 1369 cm^{-1}, C–O symmetric stretching at 1315 cm^{-1}, asymmetric stretching of C–O at 1161 cm^{-1}, C–OH skeletal vibration at 1105 cm^{-1}, pyranose C–O–C stretching at 1050 cm^{-1}, and deformation vibrations out of the plane of the aromatic ring at 896 cm^{-1}, respectively [29]. In the spectrum of PANI: PSS, the bands at 1556 cm^{-1}, and 1483 cm^{-1} correspond to C═C stretching vibrations of the quinoid and benzenoid rings, respectively. The peak presented at 1290 cm^{-1} is assigned to C–N stretching of secondary aromatic amine. The peaks at 1108 cm^{-1}, 1029 cm^{-1}, and 1002 cm^{-1} belong to the benzene ring in-plane vibration. The absorption peak at 663 cm^{-1} is due to the C–S stretching vibration of the benzene ring of PSS [30–32]. The FTIR spectrum analysis confirmed the successful

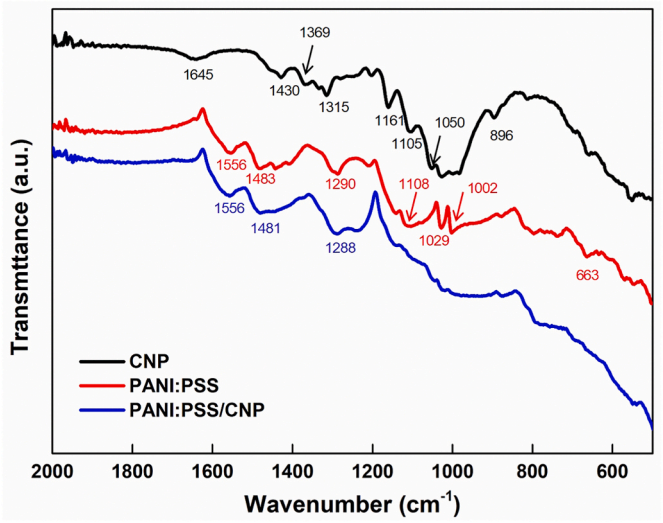

Fig. 1. FTIR spectra of CNP, PANI: PSS, and PANI: PSS/CNP.

doping of PSS into PANI. As shown in the spectrum of PANI: PSS/CNP, typical characteristic peaks of PANI: PSS (C═C (quinoid rings), C═C (benzenoid rings), and C–N) are observed, and the cellulose peaks almost disappear, indicating that PANI: PSS is uniformly coated on the CNFs surface. Furthermore, compared with the spectrum of PANI: PSS, the peaks of PANI: PSS/CNP is slightly shifted to low frequencies, which can be attributed to the formation of hydrogen bonds between CNFs and PANI: PSS. This result proves the successful synthesis of the PANI: PSS/CNP.

XPS analysis was performed to further elucidate the chemical structure of PANI: PSS/CNP. As presented in Fig. 2a, the XPS survey spectra of PANI: PSS/CNP exhibited four main peaks located at 532 eV, 399 eV, 284 eV, and 164 eV corresponding to O1s, N1s, C1s, and S2p, respectively [29,33]. The peak for N1s is from PANI, while the S2p is attributed to PSS. The N1s core-level spectrum is divided into three peaks situated at 401.06 eV (– N^+ –), 399.81 eV (– NH –), and 398.88 eV (– N═), respectively (Fig. 2b) [34,35]. Additionally, the ratio of N^+/N is 50.6% indicating a high N-doping level of PANI, which is beneficial to improving the pseudocapacitive performance of electrodes [36].

The morphology of pure CNP and PANI: PSS/CNP was investigated by SEM. As shown in Fig. 3a, the surface of pure CNP was smooth and showed an entangled nanofiber network. The cross-sectional images displayed a lamellar structure formed by CNFs tightly entangled with each other through the strong hydrogen bonding (Fig. 3b and c). CNP with a compact multilayer configuration is chosen as the flexible substrate, which is beneficial for the high mechanical properties and the fast diffusion of electrolyte ions of the electrode [37,38]. Fig. 3d confirmed that PANI: PSS particles aggregated on the surface of CNP resulting in a rougher surface of PANI: PSS/CNP after the introduction of PANI: PSS compared to pure CNP, which gived the electrode a high surface area to perform a better contact with the electrolyte [39]. Moreover, the EDS elemental mappings of carbon (C) and nitrogen (N) further demonstrated the formation of PANI: PSS on the surface of CNP (Fig. S1). The uniformly distributed PANI: PSS particles on the surface of CNF may be attributed to the hydrogen bond between the CNFs and PANI chains [40]. The expanded interior lamellar cross-sectional structures of PANI: PSS/CNP evidenced that PANI: PSS particles penetrated into the substrate, not only coated on the surface of CNP. Such a structure offers the obtained electrode excellent electrical conductivity and shorts the diffusion distance of the ions, leading to high electrochemical properties.

4.2. Mechanical property

The mechanical characteristics of pure CNP and PANI: PSS/CNP was investigated by a stress-strain experiment. As shown in Fig. 4a and b, the tensile stress and strain of PANI: PSS/CNP decreased distinctly compared to pure CNP. This degraded behavior of PANI: PSS/CNP in terms of mechanical properties may be related to the disruption of the original CNF connecting network and the formation of new hydrogen bonds between PANI: PSS and CNF after the introduction of PANI: PSS. This result matches the FTIR data. It is obvious that the PANI: PSS-CNF interactions are inherently weaker than CNF–CNF, resulting in decreased mechanical properties of PANI: PSS/CNP [41–43]. Furthermore, with the increase of PANI: PSS content, the tensile strength of PANI: PSS/CNP decreases from 49.98 MPa with a fracture strain of 14.11%–14.28 MPa with a fracture strain of 6.83%. This phenomenon can be explained by the percentage reduction of the CNFs content in PANI: PSS/CNP. The higher percentage content of CNFs in the composites typically leads to more intramolecular and intermolecular hydrogen bonds among CNFs in the PANI: PSS/CNP, which endows the composites with a higher mechanical strength. Conversely, the existence of PANI: PSS will prevent the formation of a large number of hydrogen bonds and therefore lower the mechanical strength [44]. This result evidences that the number of hydrogen bonds among CNFs affects the mechanical properties of PANI: PSS/CNP. In addition, when the PANI: PSS/CNP was sliced into 10 mm wide with 0.1 mm thick strips, the sample could still lift a static load of 800 g, where the weight ratio of PANI: PSS is 54.1% in PANI: PSS/CNP. It implies that PANI: PSS/CNP has excellent mechanical strength, which enables practical applications in flexible supercapacitors.

4.3. Conductivity

Theoretically, the electrode with a high mass loading of electrically conductive material is favorable to improve the supercapacitor performance. As anticipated, when the mass ratio of PANI: PSS to PANI: PSS/CNP increases from 7.7% to 62.2%, the conductivity of PANI: PSS/CNP electrode increases from 0.008 S/cm to 1.16 S/cm (Fig. 5a). It certifies that the electrical conductivity of PANI: PSS/CNP is mainly correlated to the content of PANI: PSS. Moreover, the measured values are superior to those of the reported cellulose conductive nanopapers [45–47]. It is worth noting that we can further improve the electrode conductivity via increasing the content of PANI: PSS, nevertheless, the mechanical performance of the composite electrode will be sacrificed. In order to prepare an electrode with high conductivity and good mechanical

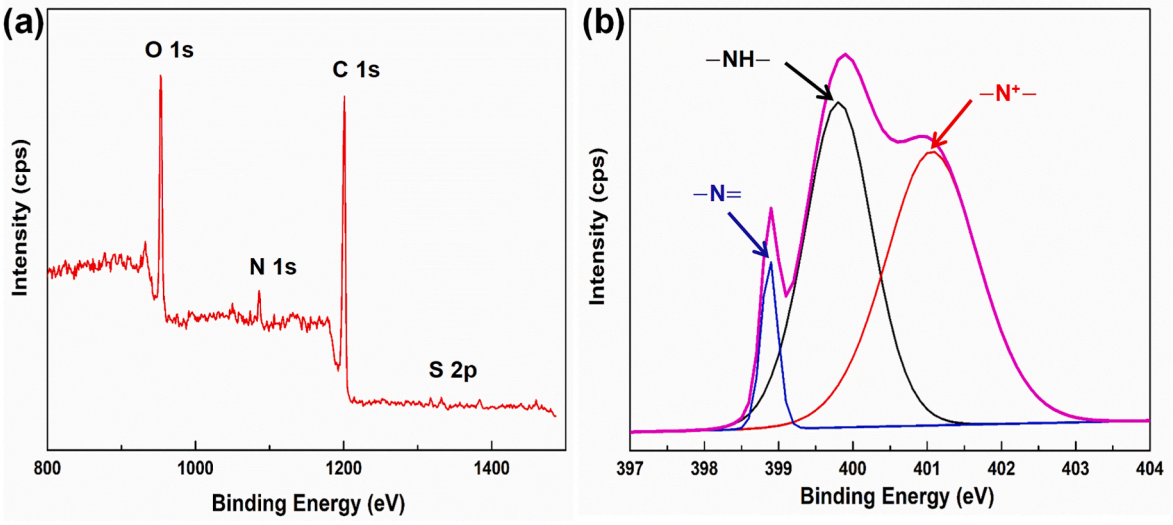

Fig. 2. (a) XPS survey spectra of PANI: PSS/CNP; (b) N1s spectra of PANI: PSS/CNP.

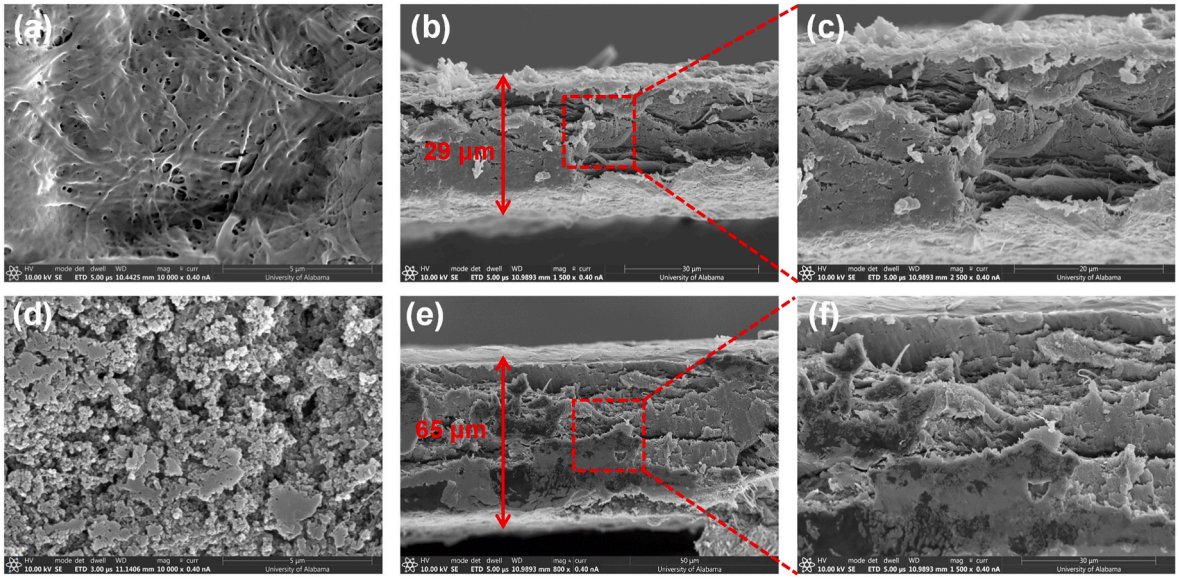

Fig. 3. (a, b, and c) SEM surface and cross-section images of pure CNP, and (d, e, and f) PANI: PSS/CNP.

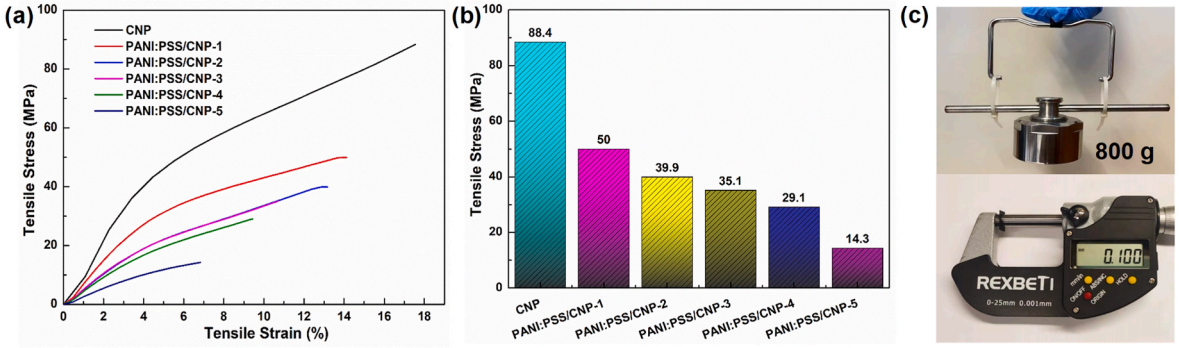

Fig. 4. (a) Stress vs. strain plot and (b) Tensile strength for CNP and PANI: PSS/CNP with different PANI: PSS mass loading; (c) Photograph of the PANI: PSS/CNP-4 strip, which could lift a static load of 800 g.

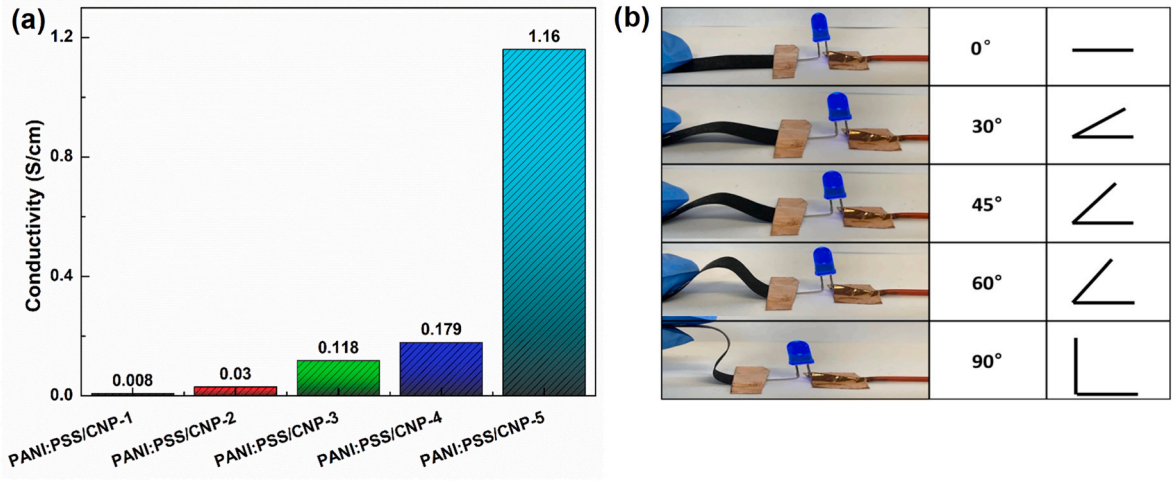

Fig. 5. (a) Conductivity and (b) Photographs of PANI: PSS/CNP-4 with different bending angles.

properties, the PANI: PSS/CNP-4 was chosen as an optimal electrode candidate and was used for the electrochemical test later. Additionally, their conductance stability and flexibility were demonstrated by maintaining the luminance of a blue LED bulb, where PANI: PSS/CNP-4 as a wire was subjected to different bending angles (Fig. 5b).

4.4. Electrochemical characterization

Fig. 6a depicted the detailed CV profiles of PANI: PSS/CNP-4 between 0 V and 0.8 V at various scan rates. The shape of curves exhibited a quasi-rectangle under lower scan rates, which was induced by the pseudocapacitive behavior of the materials. As the scan rate increased, the curve deviated from the original shape, which was attributed to the fact that electrolyte ions with finite diffusion rates couldn't diffuse from the solid/liquid interface to the electrode material and complete the electrochemical reaction at a high scan rate [48]. GCD behaviors of PANI: PSS/CNP-4 was measured at different current density. Fig. 6b showed the nearly triangular GCD curves of PANI: PSS/CNP-4 with a very small voltage drop indicating superior capacitive performance. As the current density increased, the shape of the curves was almost maintained, indicating a highly reversible charge/discharge property [49]. According to Eq. (3), the specific capacitance of the electrode derived from the GCD curves was calculated and shown in Fig. 6c and d. The maximum specific capacitance value can be obtained as high as 2.56 F/cm^2 (256 F/cm^3, 233 F/g) at 2 mA/cm^2, which is higher than other PANI-based electrode materials (Table 2). Moreover, with the increasing current density, the capacitance value obviously decreased, which was because the protons didn't have enough time to reach the surface of the electrode, which decreased the accessibility of ions and active sites resulting in low utilization of active materials. EIS was employed to analyze the ion transport behavior of PANI: PSS/CNP-4. As shown in Fig. 6e, the Nyquist plot consisted of a small semicircle in the high-frequency region presenting the charge transfer resistance and a straight line in the low-frequency region, suggesting the ideal capacitance characteristics. The cycling stability of PANI: PSS/CNP-4 was verified by GCD measurements and shown in Fig. 6f. After 8000 cycles, the specific capacitance of PANI: PSS/CNP-4 was still able to retain 81.5%. The remarkable cycling stability is ascribed to the introduction of good mechanical strength cellulose, which can more effectively prevent volume expansion/shrinkage for PANI during the charging/discharging processes. In addition, the flexibility of the electrode was evaluated by CV and GCD tests at different bending angles (0°, 90°, and 180°) (Fig. 7a–c). The result indicated that while the capacitance decreased with increasing bending angle (87% capacitance retention, at 180°), the overall stable performance demonstrated that the electrode had excellent electrochemical behavior in the bending state (Fig. 7d).

Table 2
Comparison of PANI: PSS/CNP electrode with other PANI-based electrode materials.

Electrode materials	Specific capacitance	Capacitance retention (Cycles)	Ref
CNF/CNT/PANI	315 F/g, at 1 A/g	10000, 92.0%	[50]
CNFs/MWCNTs/PANI	207.2 F/g, at 0.2 A/g	1000, 82.4%	[51]
MnS/GO/PANI	773 F/g, at 1 A/g	1000, 95.6%	[52]
graphene/PANI fiber	871.4 mF/cm^2, at 0.5 mA/cm^2	5000, 85.5%	[53]
GO/PANI/$CuCo_2O_4$	312.7 F/g, at 1 A/g	5000, 84.2%	[54]
SWCNT/cellulose/PANI	330 mF/cm^2, at 0.2 mA/cm^2	1000, 79.0%	[55]
NiO/PANI:PSS	834 F/g, at 1 A/g	3000, 88.9%	[56]
PANI:PSS/Fe-modified graphene	768.6 F/g, at 1A/g	1600, 84.0%	[14]
MWCNTs/PANI/PSS-GR	602.5 F/g, at 0.5 A/g	2000, 78.32%	[15]
PANI:PSS/CNP	2.56 F/cm^2 (256 F/cm^3, 233 F/g) at 2 mA/cm^2	8000, 81.5%	**This work**

To better understand the underlying mechanism for the improved performance of the PANI: PSS/CNP electrode, a symmetric supercapacitor was fabricated with two pieces of PANI: PSS/CNP-4 (1 cm × 1 cm × 0.10 mm, 11 mg). The electrochemical performance of the device was evaluated in the two-electrode system. Fig. 8a exhibited the CV curves of the device at different scan rates. As the scan rate increased, the CV curves of the device showed no noticeable change, suggesting an excellent rate feature and good reversibility. The GCD curves demonstrated a near triangle shape indicating the ideal capacitive property. As the current density increased, the GCD curves maintained their original shape, matching the CV results (Fig. 8b). The specific capacitance based on area, volume, and weight was calculated from the GCD curves and presented in Fig. 8c and d. The device could deliver the maximum areal capacitance of 460 mF/cm^2 (46 F/cm^3, 20.8 F/g) at 0.25 mA/cm^2. The cycling performance of the symmetric supercapacitor exhibited 78.3% capacitance retention after 2000 cycles at 2 mA/cm^2 (Fig. 8e). To estimate the specific energy and power density of the device, the corresponding ragone plot was exhibited in Fig. 9a and b. The device offered a maximum energy density of 40.9 μWh/cm^2 (4.09 mWh/cm^3) with a

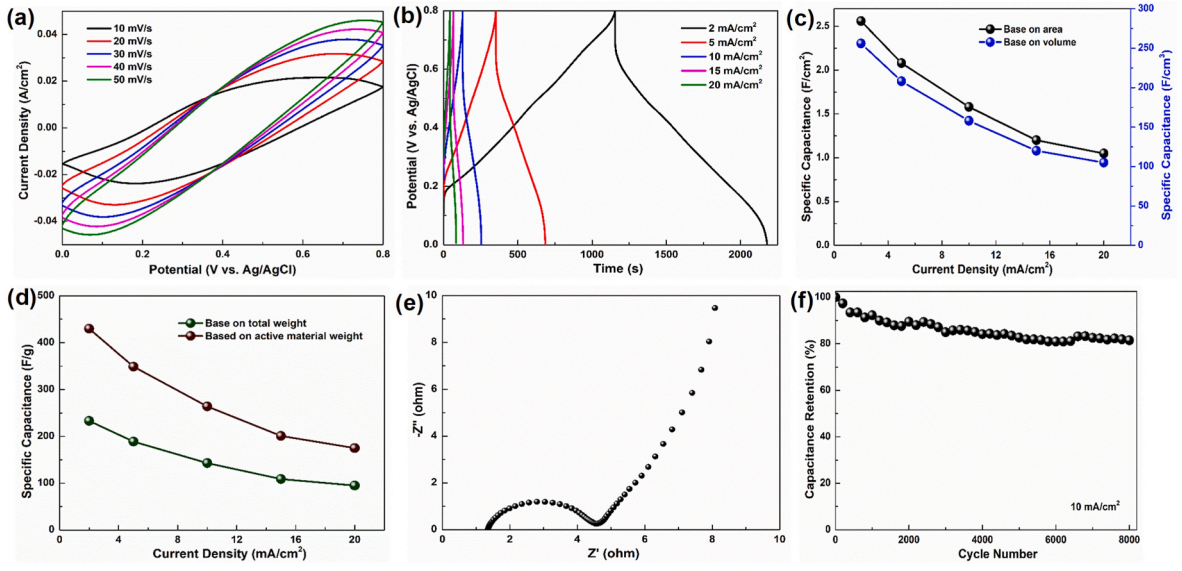

Fig. 6. The electrochemical performance of PANI: PSS/CNP-4 in 1 M H_2SO_4 electrolyte. (a) CV curves; (b) GCD curves; (c) Specific capacitance based on areal and volume as a function of current density; (d) Specific capacitance based on total weight and active material weight as a function of current density; (e) Nyquist plot; (f) Cycling stability at 10 mA/cm^2.

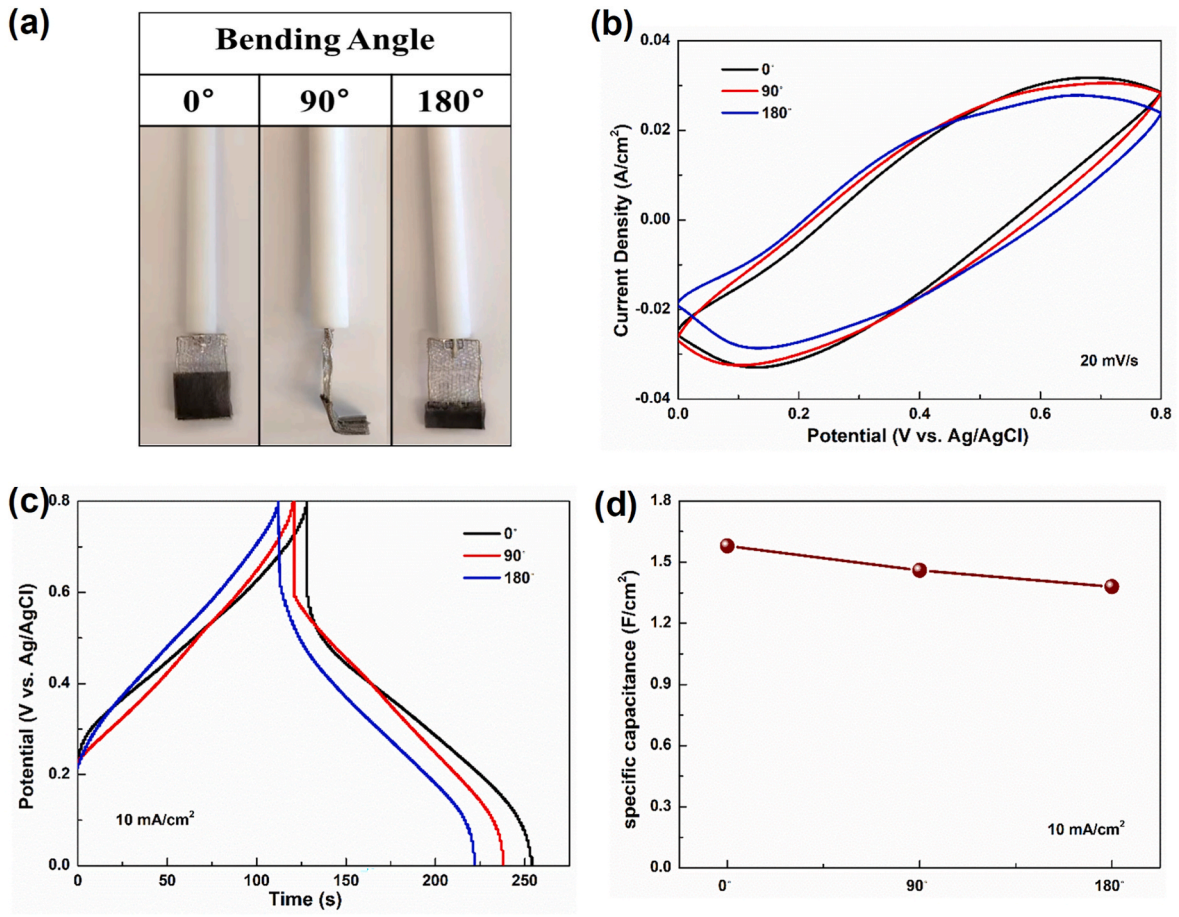

Fig. 7. (a) Digital photos of PANI: PSS/CNP-4 at different bending angles (0°, 90°, and 180°), (b) CV curves, (c) GCD curves, and (d) Specific capacitance of PANI: PSS/CNP-4 at different bending angles under 10 mA/cm^2.

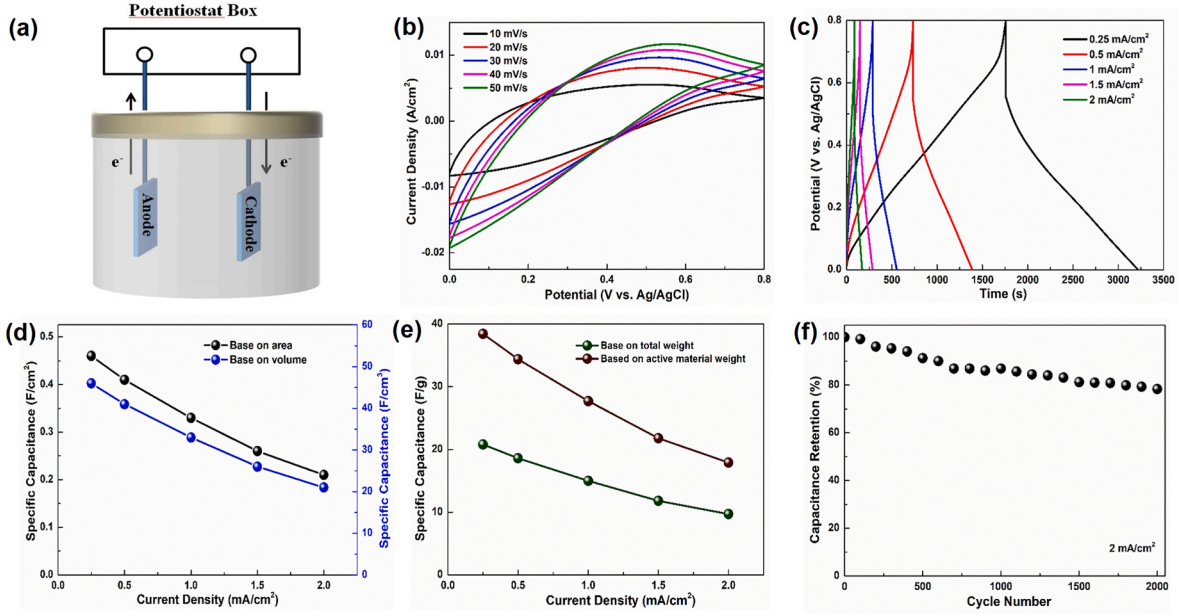

Fig. 8. (a) Schematic illustration of the PANI: PSS/CNP supercapacitor device, (b) CV curves at different scan rates; (c) GCD curves at different current density; (d) Specific capacitance based on area and volume; (e) Specific capacitance based on total weight and active material weight; (f) Cycling stability of PANI: PSS/CNP device at 2 mA/cm^2.

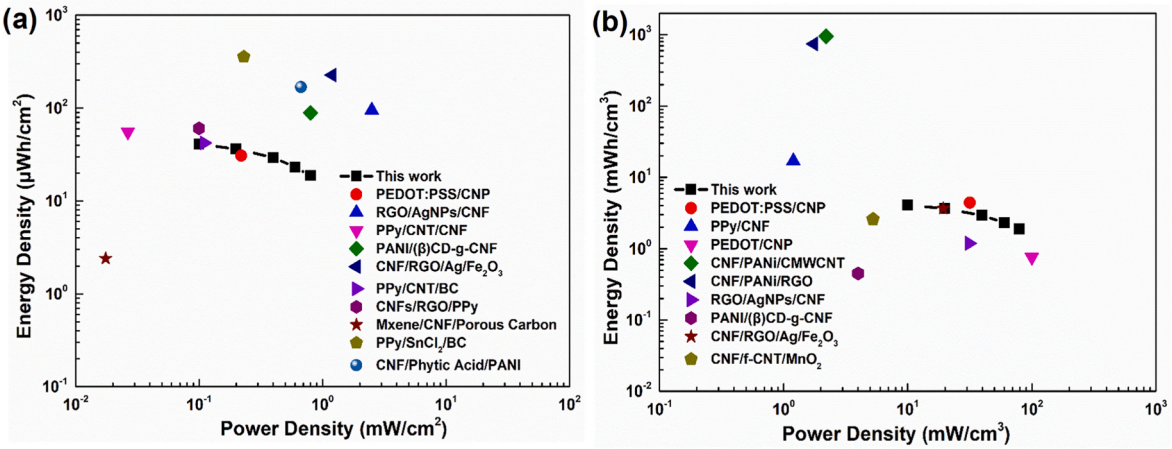

Fig. 9. Ragone plots the symmetrical PANI: PSS/CNP supercapacitor device based on (a) area and (b) volume in comparison to other cellulose materials.

power density of 100.5 μW/cm^2 (10.05 mW/cm^3), which outperformed most reported cellulose materials [26,39,49,57–66]. This result suggests that PANI: PSS/CNP is a really promising candidate material for device applications of flexible wearable energy storage.

5. Conclusion

In summary, a new freestanding, binder-free flexible PANI: PSS/CNF nanopaper electrode has been successfully fabricated by combining in situ polymerization with a simple and fast vacuum filtration method. Due to the effective combination of the cellulose as the flexible substrate and PANI: PSS as the active material, the PANI: PSS/CNP electrode exhibited high mechanical strength, good conductance stability, and superior flexibility. Besides, the PANI: PSS/CNP electrode yielded a high specific capacitance of 2.56 F/cm^2 (256 F/cm^3, 233 F/g) and good cycling stability (81.5% capacitance retention rate, 8000 cycles). Furthermore, the PANI: PSS/CNP-based symmetric supercapacitor showed a high areal energy density of 40.9 μWh/cm^2 at a power density of 100.5 μW/cm^2. It is worth noting that PANI: PSS/CNP may function well as a flexible supercapacitor electrode material because 1) PSS served as a dopant forming a water-soluble copolymer (PANI: PSS) with PANI effectively improving the processability problems of PANI, as well as a surfactant to improve the dispersity of PANI; 2) PANI with high conductivity provides good electrochemical properties (high specific capacitance, long cycling life, high power density, and energy density) to the electrode; 3) Cellulose is chosen as the flexible substrate, which provides good flexibility and mechanical strength for the electrodes due to the abundance of hydrogen bonds among cellulose molecules. Compared to conventional "rigid" electronic devices, our work provides new insight into the development of low-cost and energy-efficient flexible electrodes for the future design of green electronics.

CRediT authorship contribution statement

Yue Liang: Experimental design, Investigation, Formal analysis, Writing – original draft. **Zhen Wei:** Investigation, Writing – review & editing. **Hung-En Wang:** Experimental design, Investigation, Formal analysis. **Martin Flores:** Experimental design, Formal analysis.

Declaration of competing interest

The authors declare the following financial interests/personal relationships which may be considered as potential competing interests: Xinyu zhang reports financial support was provided by National Science Foundation. Yue liang reports financial support was provided by China Scholarship Council.

Data availability

No data was used for the research described in the article.

Acknowledgment

This work was partially supported by NSF CMMI-2113948, Yue Liang acknowledged the financial support from the China Scholarship Council (No. 201708510080).

Appendix A. Supplementary data

Supplementary data to this article can be found online at https://doi.org/10.1016/j.jpowsour.2022.232071.

References

[1] Z. Wei, J. Li, Y. Wang, R. Wang, High-performance Li-S batteries enabled by polysulfide-infiltrated free-standing 3D carbon cloth with CeO_2 nanorods decoration, Electrochim. Acta 388 (2021), 138645.
[2] Z. Wei, J. Li, R. Wang, Surface engineered polar CeO_2-based cathode host materials for immobilizing lithium polysulfides in High-performance Li-S batteries, Appl. Surf. Sci. 580 (2022), 152237.
[3] Z. Wei, R. Wang, Chemically etched CeO_2-x nanorods with abundant surface defects as effective cathode additive for trapping lithium polysulfides in Li-S batteries, J. Colloid Interface Sci. 615 (2022) 527–542.
[4] S. Azam, Z. Wei, R. Wang, Cerium oxide nanorods anchored on carbon nanofibers derived from cellulose paper as effective interlayer for lithium sulfur battery, J. Colloid Interface Sci. 615 (2022) 417–431.
[5] P. Xie, W. Yuan, X. Liu, Y. Peng, Y. Yin, Y. Li, et al., Advanced carbon nanomaterials for state-of-the-art flexible supercapacitors, Energy Storage Mater. 36 (2021) 56.
[6] M.R. Benzigar, V.D.B.C. Dasireddy, X. Guan, T. Wu, G. Liu, Advances on emerging materials for flexible supercapacitors: current trends and beyond, Adv. Funct. Mater. 30 (2020), 2002993.
[7] M. Zhang, H. Du, Z. Wei, X. Zhang, R. Wang, Ultrafast microwave synthesis of nickel-cobalt sulfide/graphene hybrid electrodes for high-performance asymmetrical supercapacitors, ACS Appl. Energy Mater. 4 (2021) 8262–8274.
[8] M. Zhang, H. Du, Z. Wei, X. Zhang, R. Wang, Facile electrodeposition of Mn-CoP nanosheets on Ni foam as high-rate and ultrastable electrodes for supercapacitors, ACS Appl. Energy Mater. 5 (2021) 186–195.
[9] M. Zhang, A. Nautiyal, H. Du, Z. Wei, X. Zhang, R. Wang, Electropolymerization of polyaniline as high-performance binder free electrodes for flexible supercapacitor, Electrochim. Acta 376 (2021), 138037.
[10] P. Liu, J. Yan, Z. Guang, Y. Huang, X. Li, W. Huang, Recent advancements of polyaniline-based nanocomposites for supercapacitors, J. Power Sources 424 (2019) 108.
[11] J. Banerjee, K. Dutta, M.A. Kader, S.K. Nayak, An overview on the recent developments in polyaniline-based supercapacitors, Polym. Adv. Technol. 30 (2019) 1902.
[12] R. Malik, S. Lata, R.S. Malik, Electrochemical behavior of composite electrode based on sulphonated polymeric surfactant (SPEEK/PSS) incorporated polypyrrole for supercapacitor, J. Electroanal. Chem. 835 (2019) 48.
[13] K. Lee, H. Yu, J.W. Lee, J. Oh, S. Bae, S.K. Kim, et al., Efficient and moisture-resistant hole transport layer for inverted perovskite solar cells using solution-processed polyaniline, J. Mater. Chem. C 6 (2018) 6250.

[14] G.E. Fenoy, B. Van der Schueren, J. Scotto, F. Boulmedais, M.R. Ceolín, S. Bégin-Colin, et al., Layer-by-layer assembly of iron oxide-decorated few-layer graphene/PANI: PSS composite films for high performance supercapacitors operating in neutral aqueous electrolytes, Electrochim. Acta 283 (2018) 1178.

[15] R. Zhang, J. Qian, S. Ye, Y. Zhou, Z. Zhu, Enhanced electrochemical capacitive performance of "sandwich-like" MWCNTs/PANI/PSS-GR electrode materials, RSC Adv. 6 (2016), 100954.

[16] K. Gholami Laelabadi, R. Moradian, I. Manouchehri, One-step fabrication of flexible, cost/time effective, and high energy storage reduced graphene oxide@PANI supercapacitor, ACS Appl. Energy Mater. 3 (2020) 5301.

[17] G.-T. Xia, C. Li, K. Wang, L.-W. Li, Structural design and electrochemical performance of PANI/CNTs and MnO_2/CNTs supercapacitor, Sci. Adv. Mater. 11 (2019) 1079.

[18] S. Anand, M.W. Ahmad, A.K.A. Al Saidi, D.-J. Yang, A. Choudhury, Polyaniline nanofiber decorated carbon nanofiber hybrid mat for flexible electrochemical supercapacitor, Mater. Chem. Phys. 254 (2020), 123480.

[19] M.S. Lakshmi, S.M. Wabaidur, Z.A. Alothman, D. Ragupathy, Novel 1D polyaniline nanorods for efficient electrochemical supercapacitors: a facile and green approach, Synth. Met. 270 (2020), 116591.

[20] H. Xu, Y. Zhu, M. Zhang, Q. Li, S. Zuo, Y. Chen, Eigenstate PANI-coated paper fiber with graphene materials for high-performance supercapacitor, Ionics 26 (2020) 5199.

[21] T. Hao, W. Wang, D. Yu, A flexible cotton-based supercapacitor electrode with high stability prepared by multiwalled CNTs/PANI, J. Electron. Mater. 47 (2018) 4108.

[22] T. Li, C. Chen, A.H. Brozena, J.Y. Zhu, L. Xu, C. Driemeier, et al., Developing fibrillated cellulose as a sustainable technological material, Nature 590 (2021) 47.

[23] A. Sharma, M. Thakur, M. Bhattacharya, T. Mandal, S. Goswami, Commercial application of cellulose nano-composites-A review, Biotechnol. Rep. 21 (2019), e00316.

[24] L. Deng, R.J. Young, I.A. Kinloch, A.M. Abdelkader, S.M. Holmes, D.A. De Haro-Del Rio, et al., Supercapacitance from cellulose and carbon nanotube nanocomposite fibers, ACS Appl. Mater. Interfaces 5 (2013) 9983.

[25] M. Mo, C. Chen, H. Gao, M. Chen, D. Li, Wet-spinning assembly of cellulose nanofibers reinforced graphene/polypyrrole microfibers for high performance fiber-shaped supercapacitors, Electrochim. Acta 269 (2018) 11.

[26] H. Du, M. Zhang, K. Liu, M. Parit, Z. Jiang, X. Zhang, et al., Conductive PEDOT: PSS/cellulose nanofibril paper electrodes for flexible supercapacitors with superior areal capacitance and cycling stability, Chem. Eng. J. 428 (2022), 131994.

[27] M. Parit, H. Du, X. Zhang, C. Prather, M. Adams, Z. Jiang, Polypyrrole and cellulose nanofiber based composite films with improved physical and electrical properties for electromagnetic shielding applications, Carbohydr. Polym. 240 (2020), 116304.

[28] L. Wang, T. Shu, S. Guo, Y. Lu, M. Li, J. Nzabahimana, et al., Fabricating strongly coupled V_2O_5@PEDOT nanobelts/graphene hybrid films with high areal capacitance and facile transferability for transparent solid-state supercapacitors, Energy Storage Mater. 27 (2020) 150.

[29] C. Wan, Y. Jiao, J. Li, Flexible, highly conductive, and free-standing reduced graphene oxide/polypyrrole/cellulose hybrid papers for supercapacitor electrodes, J. Mater. Chem. 5 (2017) 3819.

[30] S. Uzunçar, L. Meng, A.P.F. Turner, W.C. Mak, Processable and nanofibrous polyaniline: polystyrene-sulphonate (nano-PANI: PSS) for the fabrication of catalyst-free ammonium sensors and enzyme-coupled urea biosensors, Biosens. Bioelectron. 171 (2021), 112725.

[31] P. Ranka, V. Sethi, A.Q. Contractor, One step electrodeposition of composite of PANI-PSS tubules with TiO_2 nanoparticles and application as electronic sensor device, Sensor. Actuator. B Chem. 261 (2018) 11.

[32] S. Biswas, J. Jeong, J.W. Shim, H. Kim, Improved charge transport in PANI: PSS by the uniform dispersion of silver nanoparticles, Appl. Surf. Sci. 483 (2019) 819.

[33] H. Han, J.S. Lee, S. Cho, Comparative studies on two-electrode symmetric supercapacitors based on polypyrrole: poly (4-styrenesulfonate) with different molecular weights of poly (4-styrenesulfonate), Polymers 11 (2019) 232.

[34] A.D.W. Carswell, E.A. O'Rea, B.P. Grady, Adsorbed surfactants as templates for the synthesis of morphologically controlled polyaniline and polypyrrole nanostructures on flat surfaces: from spheres to wires to flat films, J. Am. Chem. Soc. 125 (2003), 14793.

[35] G.M. do Nascimento, V.R.L. Constantino, R. Landers, M.L.A. Temperini, Spectroscopic characterization of polyaniline formed in the presence of montmorillonite clay, Polymer 47 (2006) 6131.

[36] Y. Li, Z. Xia, Q. Gong, X. Liu, Y. Yang, C. Chen, et al., Green synthesis of free standing cellulose/graphene oxide/polyaniline aerogel electrode for high-performance flexible all-solid-state supercapacitors, Nanomaterials 10 (2020) 1546.

[37] J.P. Jyothibasu, D.-W. Kuo, R.-H. Lee, Flexible and freestanding electrodes based on polypyrrole/carbon nanotube/cellulose composites for supercapacitor application, Cellulose 26 (2019) 4495.

[38] H. Xu, Y. Li, M. Jia, L. Cui, C. Chen, Y. Yang, et al., Design and synthesis of a 3D flexible film electrode based on a sodium carboxymethyl cellulose-polypyrrole@reduced graphene oxide composite for supercapacitors, New J. Chem. 45 (2021) 6630.

[39] W. Wang, Y. Yang, Z. Chen, Z. Deng, L. Fan, W. Guo, et al., High-performance yarn supercapacitor based on directly twisted carbon nanotube@bacterial cellulose membrane, Cellulose 27 (2020) 7649.

[40] T. Wang, W. Zhang, S. Yang, X. Liu, L. Zhang, Preparation of foam-like network structure of polypyrrole/graphene composite particles based on cellulose nanofibrils as electrode material, ACS Omega 5 (2020) 4778.

[41] G. Nystrom, A. Mihranyan, A. Razaq, T. Lindstrom, L. Nyholm, M. Strømme, A nanocellulose polypyrrole composite based on microfibrillated cellulose from wood, J. Phys. Chem. B 114 (2010) 4178.

[42] Y. Zhang, T. Nypelö, C. Salas, Cellulose nanofibrils: from strong materials to bioactive surfaces, J Renew Mater 1 (2013) 195–211.

[43] D. Zhang, Q. Zhang, X. Gao, G. Piao, A nanocellulose polypyrrole composite based on tunicate cellulose, Int. J. Polym. Sci. 2013 (2013) 1687.

[44] S.S. Nair, N. Yan, Effect of high residual lignin on the thermal stability of nanofibrils and its enhanced mechanical performance in aqueous environments, Cellulose 22 (2015) 3137.

[45] M. Parit, H. Du, X. Zhang, C. Prather, M. Adams, Z. Jiang, Polypyrrole and cellulose nanofiber based composite films with improved physical and electrical properties for electromagnetic shielding applications, Carbohydr. Polym. 240 (2020), 116304.

[46] M. Lay, J.A. Méndez, M. Pèlach, K.N. Bun, F. Vilaseca, Combined effect of carbon nanotubes and polypyrrole on the electrical properties of cellulose-nanopaper, Cellulose 23 (2016) 3925.

[47] Y. Li, H. Zhang, S. Ni, H. Xiao, In situ synthesis of conductive nanocrystal cellulose/polypyrrole composite hydrogel based on semi-interpenetrating network, Mater. Lett. 232 (2018) 175.

[48] M. Salado, S. Lanceros-Mendez, E. Lizundia, Free-standing intrinsically conducting polymer membranes based on cellulose and poly (vinylidene fluoride) for energy storage applications, Eur. Polym. J. 144 (2021), 110240.

[49] Q. Fu, Y. Wang, S. Liang, Q. Liu, C. Yao, High-performance flexible freestanding polypyrrole-coated CNF film electrodes for all-solid-state supercapacitors, J. Solid State Electrochem. 24 (2020) 533.

[50] F. Miao, C. Shao, X. Li, K. Wang, N. Lu, Y. Liu, Electrospun carbon nanofibers/carbon nanotubes/polyaniline ternary composites with enhanced electrochemical performance for flexible solid-state supercapacitors, ACS Sustain. Chem. Eng. 4 (2016) 1689.

[51] C. Yang, D. Li, Flexible and foldable supercapacitor electrodes from the porous 3D network of cellulose nanofibers, carbon nanotubes and polyaniline, Mater. Lett. 155 (2015) 78.

[52] K.Y. Yasoda, S. Kumar, M.S. Kumar, K. Ghosh, S.K. Batabyal, Fabrication of MnS/GO/PANI nanocomposites on a highly conducting graphite electrode for supercapacitor application, Mater. Today Chem. 19 (2021), 100394.

[53] L. Qin, G. Yang, D. Li, K. Ou, H. Zheng, Q. Fu, et al., High area energy density of all-solid-state supercapacitor based on double-network hydrogel with high content of graphene/PANI fiber, Chem. Eng. J. 430 (2022), 133045.

[54] S. Verma, V.K. Pandey, B. Verma, Facile synthesis of graphene oxide-polyaniline-copper cobaltite (GO/PANI/$CuCo_2O_4$) hybrid nanocomposite for supercapacitor applications, Synth. Met. 286 (2022), 117036.

[55] D. Ge, L. Yang, L. Fan, C. Zhang, X. Xiao, Y. Gogotsi, et al., Foldable supercapacitors from triple networks of macroporous cellulose fibers, single-walled carbon nanotubes and polyaniline nanoribbons, Nano Energy 11 (2015) 568.

[56] E.-C. Cho, C.-W. Chang-Jian, K.-C. Lee, J.-H. Huang, B.-C. Ho, Y.-R. Ding, et al., Spray-dried nanoporous NiO/PANI: PSS composite microspheres for high-performance asymmetric supercapacitors, Compos. B Eng. 175 (2019), 107066.

[57] J.P. Jyothibasu, R.-H. Wang, K. Ong, J.H.L. Ong, R.-H. Lee, Cellulose/carbon nanotube/MnO_2 composite electrodes with high mass loadings for symmetric supercapacitors, Cellulose 28 (2021) 3549.

[58] Y. Sun, Y. Yang, L. Fan, W. Zheng, D. Ye, J. Xu, Polypyrrole/$SnCl_2$ modified bacterial cellulose electrodes with high areal capacitance for flexible supercapacitors, Carbohydr. Polym. (2022) 119679.

[59] W. Chen, D. Zhang, K. Yang, M. Luo, P. Yang, X. Zhou, Mxene ($Ti_3C_2T_x$)/cellulose nanofiber/porous carbon film as free-standing electrode for ultrathin and flexible supercapacitors, Chem. Eng. J. 413 (2021), 127524.

[60] Y. Zhang, Z. Shang, M. Shen, S.P. Chowdhury, A. Ignaszak, S. Sun, et al., Cellulose nanofibers/reduced graphene oxide/polypyrrole aerogel electrodes for high-capacitance flexible all-solid-state supercapacitors, ACS Sustain. Chem. Eng. 7 (2019), 11175.

[61] A. Lu, H. Wan, C. Qin, Flexible, robust cellulose/phytic acid/polyaniline hydrogel for all-in-one supercapacitor and strain sensor, J. Mater. Chem. 10 (2022) 17279–17287.

[62] Z. Zou, W. Xiao, Y. Zhang, H. Yu, W. Zhou, Facile synthesis of freestanding cellulose/RGO/silver/Fe_2O_3 hybrid film for ultrahigh-areal-energy-density flexible solid-state supercapacitor, Appl. Surf. Sci. 500 (2020), 144244.

[63] Q. Gong, Y. Li, X. Liu, Z. Xia, Y. Yang, A facile preparation of polyaniline/cellulose hydrogels for all-in-one flexible supercapacitor with remarkable enhanced performance, Carbohydr. Polym. 245 (2020), 116611.

[64] Z. Zou, W. Zhou, Y. Zhang, H. Yu, C. Hu, W. Xiao, High-performance flexible all-solid-state supercapacitor constructed by free-standing cellulose/reduced graphene oxide/silver nanoparticles composite film, Chem. Eng. J. 357 (2019) 45.

[65] S. Lyu, Y. Chen, L. Zhang, S. Han, Y. Lu, Y. Chen, et al., Nanocellulose supported hierarchical structured polyaniline/nanocarbon nanocomposite electrode via layer-by-layer assembly for green flexible supercapacitors, RSC Adv. 9 (2019), 17824.

[66] B. Li, H. Lopez-Beltran, C. Siu, K.H. Skorenko, H. Zhou, W.E. Bernier, et al., Vaper phase polymerized PEDOT/cellulose paper composite for flexible solid-state supercapacitor, ACS Appl. Energy Mater. 3 (2020) 1559.